

# Materials Advances

Accepted Manuscript

This article can be cited before page numbers have been issued, to do this please use: T. K. C. Phu, N. Nguyen, P. L. NGUYEN, N. N. Le and T. V. B. Phung, *Mater. Adv.*, 2026, DOI: 10.1039/D6MA00391E.



This is an Accepted Manuscript, which has been through the Royal Society of Chemistry peer review process and has been accepted for publication.

Accepted Manuscripts are published online shortly after acceptance, before technical editing, formatting and proof reading. Using this free service, authors can make their results available to the community, in citable form, before we publish the edited article. We will replace this Accepted Manuscript with the edited and formatted Advance Article as soon as it is available.

You can find more information about Accepted Manuscripts in the [Information for Authors](#).

Please note that technical editing may introduce minor changes to the text and/or graphics, which may alter content. The journal's standard [Terms & Conditions](#) and the [Ethical guidelines](#) still apply. In no event shall the Royal Society of Chemistry be held responsible for any errors or omissions in this Accepted Manuscript or any consequences arising from the use of any information it contains.

## Electrochemical behavior of rapid-synthesized amorphous aerogel 3d-VIII B-metal aerogels as bifunctional electrocatalysts for water splitting

Thi Kim Cuong Phu,<sup>a</sup> Ngoc-Trung Nguyen,<sup>a</sup> Phi Long Nguyen,<sup>a,b</sup> Ngan Nguyen Le,<sup>c,d\*</sup> and Thi Viet Bac Phung<sup>a,e\*</sup>

<sup>a</sup> Center for Environmental Intelligence, VinUniversity, Hanoi, Vietnam

<sup>b</sup> School of Electrical and Electronic Engineering, Hanoi University of Industry, Hanoi, Vietnam

<sup>c</sup> Institute of Applied Science and Technology, Van Lang School of Technology, Van Lang University, Ho Chi Minh City, Vietnam

<sup>d</sup> Faculty of Applied Technology, Van Lang School of Technology, Van Lang University, Ho Chi Minh City, Vietnam

<sup>e</sup> College of Engineering and Computer Science, VinUniversity, Hanoi, Vietnam

### \*Corresponding author:

Thi Viet Bac Phung; E-mail: [bac.ptv@vinuni.edu.vn](mailto:bac.ptv@vinuni.edu.vn)

Ngan Nguyen Le; E-mail: [ngan.ln@vlu.edu.vn](mailto:ngan.ln@vlu.edu.vn)



## Abstract

Oxygen vacancies ( $O_V$ ) in metal oxide electrocatalysts are broadly regarded as pivotal factors that improve electrochemical catalytic efficiency in water splitting. However, the intrinsic properties of catalysts also play an important role in the overall catalytic performance. Here, we present the facile synthesis and investigate the interplay between  $O_V$  content and intrinsic properties as bifunctional electrocatalysts for hydrogen evolution reaction (HER) and oxygen evolution reaction (OER). Despite being derived from the same class of metal (II) chloride precursors, the three aerogels exhibit distinctly different amorphous porous architectures: sphere-like particles (Fe), flower-like hierarchical nanosheets (Co), and densely packed ultrasmall spheres (Ni). Among the three,  $O_V$ -rich Co aerogel stands out due to a synergistic combination of the highest  $O_V$  percentage (89.4%), the largest specific surface area ( $134.5 \text{ m}^2 \text{ g}^{-1}$ ), and favorable intrinsic electronic properties of the Co center, which together maximize active site density and facilitate efficient charge transfer for both HER and OER intermediates. Consequently, Co aerogel delivers outstanding bifunctional performance with overpotentials of only 383 mV (OER) and 365 mV (HER) at  $100 \text{ mA cm}^{-2}$  in alkaline electrolyte, along with long-term durability over 70 h. Importantly, despite possessing substantial  $O_V$  content, Fe and Ni aerogels exhibit negligible or poor catalytic activity in neutral electrolyte, demonstrating that  $O_V$  content alone is insufficient, and intrinsic material properties are equally decisive in governing electrocatalytic performance. This study thus provides mechanistic insights into the relative contributions of  $O_V$  and intrinsic properties in water splitting electrocatalysis, alongside a scalable synthesis route for high-performance Co-based aerogel electrocatalysts.



## 1. Introduction

Water splitting enabled by renewable energy sources represents a promising strategy for sustainable hydrogen production, contributing to climate change mitigation and reducing dependence on fossil fuels.<sup>1</sup> However, the sluggish kinetics of HER and OER significantly hinder the efficiency of water splitting.<sup>2-4</sup> Currently, Pt/C and IrO<sub>2</sub> are considered the most efficient HER and OER electrocatalysts, respectively, yet their high costs and limited reserves hinder their large-scale application.<sup>5</sup> Consequently, developing non-noble HER and OER catalysts is essential for large-scale industrial applications.<sup>6</sup> As most promising electrocatalysts for anodic OER and cathodic HER, endowed with abundance and proven high-performance, 3d-VIIIB-based catalysts have been remarkably investigated as alternatives to noble metals.<sup>7-10</sup> Extensive studies have demonstrated that amorphous electrocatalysts generally exhibit superior catalytic performance compared to their crystalline counterparts, primarily due to the presence of a high density of catalytically active sites.<sup>11-13</sup> These abundant active sites effectively promote the transport of charged species during the electrochemical water splitting process, thereby enabling synergistic catalytic contributions from both surface and bulk regions of the catalyst.<sup>14,15</sup> Additionally, O<sub>v</sub> engineering can pave the way to accelerate catalytic performance via optimizing adsorption and desorption of intermediates and catalytic active sites.<sup>16,17</sup> Therefore, designing economical catalysts that deliver high-porous structure and large O<sub>v</sub> percentage via facile synthesis routes which is an important step for economical electrochemical water splitting.

In this work, amorphous 3d-VIIIB-metal aerogels featuring significant porous architectures and abundant O<sub>v</sub> amount were rapidly synthesized via an ambient facile reduction method, and their electrocatalytic performance toward anodic OER and cathodic HER were systematically



investigated in neutral and alkaline environments. Simultaneously, the contribution of carbon cloth (CC) as conductive substrate in HER/OER catalytic performance was systematically assessed to elucidate the intrinsic electrocatalytic activity of the as-prepared catalysts. Among as-prepared catalysts, in alkaline and neutral electrolytes, rich  $O_V$ -Co aerogel exhibits the highest OER and HER performance. Besides that, 72-h long-term stability using rich  $O_V$ -Co aerogel as working electrode shows slight degradation with  $\sim 130$  mV-decrease in alkaline OER and  $\sim 20$  mV-decrease in alkaline HER. Notably, a high  $O_V$  content alone does not guarantee superior catalytic performance; intrinsic material properties, such as the inherent electronic structure of the metal center, can play an equally decisive role. For instance, despite possessing substantial  $O_V$  content,  $O_V$ -rich Fe and  $O_V$ -rich Ni aerogels exhibit poor catalytic activity for both HER and OER in neutral electrolyte, highlighting that the interplay between  $O_V$  and intrinsic material properties governs overall electrocatalytic performance. This study therefore aims to systematically elucidate the relative contributions of  $O_V$  content and intrinsic material properties to electrocatalytic water splitting across alkaline and neutral conditions.

## 2. Experimental section

The  $O_V$ -rich Fe aerogel (after being denoted as Fe aerogel) was synthesized by mixing 200 mL of a 0.1 M iron(II) chloride tetrahydrate solution ( $FeCl_2 \cdot 4H_2O$ , CAS No. 13478-10-9, Thermo Fisher) with 400 mL of 0.1 M sodium borohydride ( $NaBH_4$ , CAS No. 16940-66-2, Weng Jiang Reagent) in a glass bottle. The resulting black suspension was vigorously shaken and then allowed to stand for 24 h. Subsequently, the Fe aerogel precipitate was collected, washed several times with deionized water, and dried overnight in a vacuum oven at 60 °C.  $O_V$ -rich Co and  $O_V$ -rich Ni aerogels (after being denoted as Co and Ni aerogels, respectively) were synthesized following the



same procedure using 200 mL of 0.1 M cobalt (II) chloride ( $\text{CoCl}_2$ , CAS No. 7646-79-7, Sigma-Aldrich) and 200 mL of 0.1 M nickel(II) chloride ( $\text{NiCl}_2$ , CAS No. 7718-54-9, Shanghai Titan Scientific Co., Ltd.) as precursors, respectively.

All electrochemical measurements were carried out using a Corrtest C@310M electrochemical workstation in a conventional three-electrode configuration. The catalyst ink was prepared by dispersing 10 mg of the synthesized catalyst in a mixed solvent of isopropanol and ethanol (1:1 v/v, total volume 0.98 mL) under ultrasonic treatment for 3 h. Subsequently, 0.02 mL of 5 wt.% Nafion solution was added, followed by an additional 1 h of sonication to obtain a uniform suspension. Then, 0.1 mL of the resulting catalyst ink was drop-cast onto a  $1 \times 1 \text{ cm}^2$  carbon cloth substrate (W0S1011) with loading of  $1 \text{ mg cm}^{-2}$  acting as working electrode. A 0.5 M phosphate buffer solution (PBS, pH 7) was prepared by dissolving 1.68 g of potassium dihydrogen phosphate ( $\text{KH}_2\text{PO}_4$ , CAS No. 7778-77-0, GHTECH) and 1.75 g of dipotassium hydrogen phosphate trihydrate ( $\text{K}_2\text{HPO}_4 \cdot 3\text{H}_2\text{O}$ , CAS No. 16788-57-1, Xilong) in 200 mL of deionized water ( $13.1 \text{ M}\Omega \text{ cm}$ ) with continuous stirring at ambient temperature until complete dissolution. A  $1 \times 1 \text{ cm}^2$  Pt plate was employed as the counter electrode. Ag/AgCl and Hg/HgO electrodes were used as reference electrodes in neutral (0.5 M PBS, pH 7) and alkaline (0.5 M KOH, pH 13.2, CAS No. 1310-58-3, Sigma-Aldrich) electrolytes, respectively.

All cyclic voltammetry (CV) curves recorded at a scan rate of  $5 \text{ mV s}^{-1}$  for anodic OER and cathodic HER tests were corrected using  $iR_s$  compensation. In contrast, no  $iR_s$  compensation was applied to the chronopotentiometric (CP) measurements. All potentials were converted to the reversible

$$E(\text{RHE}) = E(\text{Ag}/\text{AgCl}) + 0.197 \text{ V} + 0.059 \times \text{pH} - iR_s$$



$$E(\text{RHE}) = E(\text{Hg}/\text{HgO}) + 0.140 \text{ V} + 0.059 \times \text{pH} - iR_s$$

in which  $R_s$  is uncompensated resistance.

The kinetic parameters of the as-prepared electrocatalysts were evaluated by extracting Tafel slopes through linear regression of the linear portions of the corresponding Tafel curves:

$$\eta = b \log |j| + a$$

Where  $b$  and  $j$  are the Tafel slope and current density, respectively.

Electrochemical impedance spectroscopy (EIS) tests were carried out under a specific applied potential using an alternative current signal amplitude of 10 mV, a frequency range 100 kHz-0.1 Hz. The electrochemical double-layer capacitance ( $C_{dl}$ ) was evaluated using CV tests at different scan rates (2, 5, 10, 15, 20, and 25  $\text{mV s}^{-1}$ ) within the non-faradaic potential region. The  $C_{dl}$  values were extracted from the slope of the linear fit of  $S/(2 \times \Delta V)$  as a function of scan rate, where  $S$  denotes the enclosed area of the CV curve and  $\Delta V$  represents the potential window.

Phase identification of the synthesized catalysts was carried out by powder X-ray diffraction (XRD) on a Bruker D8 Advance (Cu  $K\alpha$ ,  $\lambda = 0.154 \text{ nm}$ ),  $2\theta$  window  $10^\circ - 90^\circ$  at a scanning speed of  $5^\circ \text{ min}^{-1}$ . Specific surface area and pore size were evaluated by nitrogen adsorption measurements based on the Brunauer-Emmett-Teller (BET) method using a Quantachrome NOVA Station C at 77.3 K. Morphology of obtained catalysts was investigated using a Hitachi S-4800 field emission scanning electron microscope (FE-SEM) operated at an accelerating voltage of 10.0 kV and high-resolution transmission electron microscopy (HR-TEM, JEM2100). Oxidation states of elements are characterized by Al- $K\alpha$  source X-ray photoelectron spectroscopy (XPS) (JPS-9030 Photoelectron Spectrometer) (C 1s XPS spectra with C-C peak at 284.7 eV, **Figure S1, SI**).



### 3. Results and Discussion

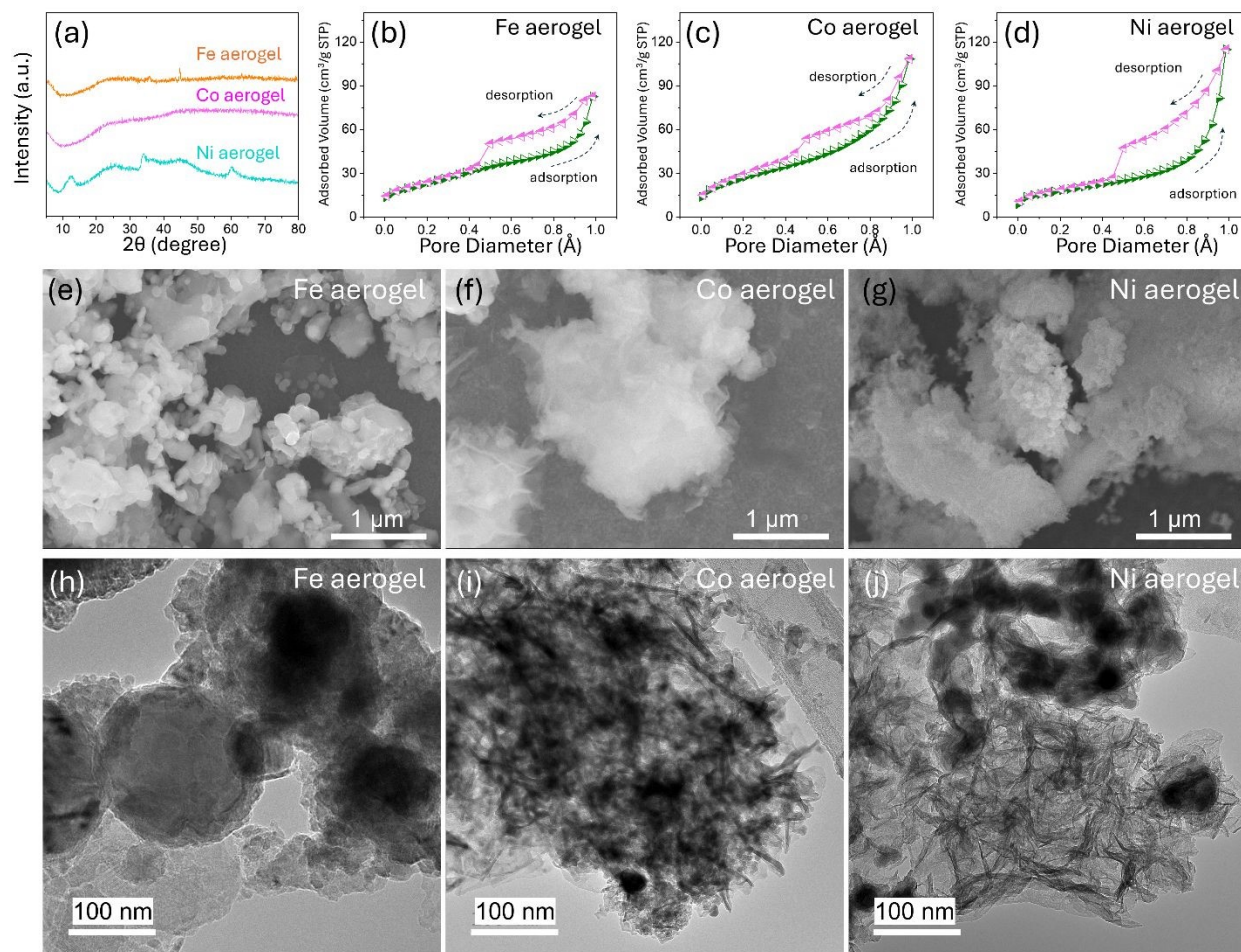


**Figure 1.** Structural and morphology characterizations of as-synthesized aerogel. a) XRD patterns. N<sub>2</sub> adsorption-desorption isotherms of b) Fe aerogel, c) Co aerogel, d) Ni aerogel. FESEM images of e) Fe aerogel, f) Co aerogel, g) Ni aerogel, and HRTEM images of h) Fe aerogel, i) Co aerogel, j) Ni aerogel.

The amorphous 3d-VIII B-based O<sub>V</sub>-rich aerogels were synthesized through a template-free self-assembly route, employing 3d-VIII B-based metal (II) chloride salts as precursors, with NaBH<sub>4</sub> serving as source of active hydrogen (H\*) reducing agent. This approach is widely employed for



the fabrication of porous metal oxide architectures.<sup>18,19</sup> In contrast to the sharp and intense diffraction peaks observed for crystalline materials, XRD patterns of the as-synthesized catalysts display a distinct broad halo, reflecting a predominantly amorphous phase with only short-range structural ordering (**Figure 1a**).<sup>20–22</sup> For the Ni aerogel, the appearance of weak yet sharp diffraction peaks could suggest the coexistence of minor crystalline domains, likely arising from incomplete precursor conversion or slight crystallization occurring during the synthesis process. Nevertheless, the preponderance of an amorphous background in the Ni aerogel confirms that the overall structure of the synthesized catalysts is primarily governed by the amorphous phase. As shown in **Figure 1b-d**, Fe, Co, and Ni aerogels exhibit H1-type hysteresis loops, characterized by a pronounced adsorption-desorption hysteresis in the relative pressure range of 0.45 - 1.0. A sharp inflection point at  $P/P_0$  of 0.5 suggests the presence of ink-bottle-type pore morphology.<sup>23</sup> Among the as-synthesized catalysts, Co aerogel exhibits the highest specific surface area ( $134.461 \text{ m}^2 \text{ g}^{-1}$ ), exceeding those of Ni aerogel ( $103.382 \text{ m}^2 \text{ g}^{-1}$ ) and Fe aerogel ( $94.128 \text{ m}^2 \text{ g}^{-1}$ ). The adsorption-desorption behavior of all as-prepared catalysts is predominantly governed by micro- and mesoporous structures, with pore sizes mainly distributed in the range of 2-50 nm (**Figure S2**, SI). The detailed adsorption-desorption parameters are summarized in **Table S1** (SI). During the reduction reaction of 3d-VIIIB-metal chloride salts, excessive amount of *in situ*-generated  $\text{H}_2$  bubbles beneficially facilitates the formation of porous structures. As shown in **Figure 1e**, the morphology of Fe aerogel exhibits irregularly aggregated and sphere-like particles which are characteristic of nanoparticles synthesized via sol-gel routes. Notably, Co aerogel exhibits a flower-like microspherical architecture assembled from numerous interleaving nanosheets (**Figure 1f**). Ni aerogel consists of densely packed and ultrasmall spherical particles (**Figure 1g**). Revealed from HR-TEM images, the sphere-like of Fe aerogel, and flower-like morphology of Co aerogel



and densely packed spherical particles intercalating with ultrathin nanoflakes of Ni aerogel are highlights further (**Figure 1h-j**). As a result, the high porous structure of as-prepared catalysts is beneficial for increasing the number of catalytic active sites, accelerating mass transfer during the catalytic process.

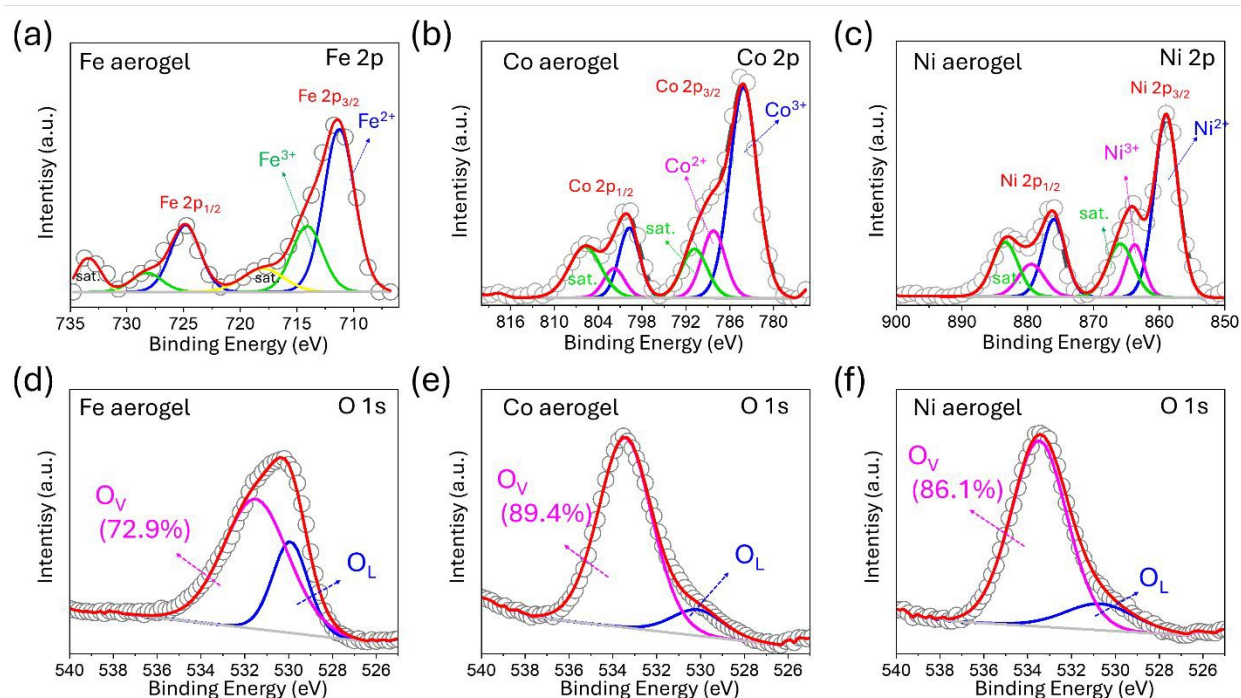


**Figure 2.** High-resolution XPS spectra for a) Fe 2p of Fe aerogel, b) Co 2p of Co aerogel, c) Ni 2p of Ni aerogel; and O 1s XPS spectra of d) Fe aerogel, e) Co aerogel, and Ni aerogel.

XPS was utilized to get insights into surface chemistry of the catalyst such as valence states and chemical composition. **Figure 2a** shows XPS spectrum of Fe 2p with peaks at 711.35 eV and 724.75 eV ascribing to Fe 2p<sub>3/2</sub> in and Fe 2p<sub>1/2</sub> which can be deconvoluted into Fe<sup>2+</sup> 2p<sub>3/2</sub> (711.21 eV), Fe<sup>3+</sup> 2p<sub>3/2</sub> (714.02 eV), Fe<sup>2+</sup> 2p<sub>1/2</sub> (724.8 eV), and Fe<sup>3+</sup> 2p<sub>1/2</sub> (728.15 eV).<sup>24,25</sup> Co 2p XPS spectra can be deconvoluted into six peaks, namely Co<sup>3+</sup> 2p<sub>3/2</sub> (784.41 eV), Co<sup>2+</sup> 2p<sub>3/2</sub> (788.61 eV), Co<sup>3+</sup> 2p<sub>1/2</sub> (799.61 eV), and Co<sup>2+</sup> 2p<sub>1/2</sub> (801.61 eV), along with a pair of satellite peaks (**Figure**



**2b).**<sup>26</sup> Similarly, the Ni 2p XPS spectrum shows peaks at 858.93 eV and 875.93 eV, corresponding to the Ni 2p<sub>3/2</sub> and Ni 2p<sub>1/2</sub> (**Figure 2c**). The Ni 2p signals of the sample can be deconvoluted into six strong peaks, namely Ni<sup>2+</sup> 2p<sub>3/2</sub> (858.93 eV), Ni<sup>3+</sup> 2p<sub>3/2</sub> (863.93 eV), Ni<sup>2+</sup> 2p<sub>1/2</sub> (875.93 eV), Ni<sup>3+</sup> 2p<sub>1/2</sub> (879.93 eV), accompanied by a pair of satellite peaks.<sup>27</sup> The mixed valence states of metals in synthesized aerogels can be beneficial for enhancing HER and OER performance. The XPS O 1s spectrum in Fe aerogel reveals two characteristic signals at ~529.9 eV and ~531.6 eV, corresponding to oxygen lattice (O<sub>L</sub>) and oxygen vacancy (O<sub>V</sub>), respectively (**Figure 2d**).<sup>28,29</sup> As shown in **Figure 2e-f**, in Co and Ni aerogels, O<sub>L</sub> and O<sub>V</sub> characteristic peaks can be identified at ~230 eV and ~533 eV, respectively. Among O<sub>V</sub>-rich aerogels, Co aerogel exhibits the highest O<sub>V</sub> percentage (89.4%) compared to Ni aerogel (86.1%) and Fe aerogel (72.9%). The introduction of oxygen vacancies can facilitate charge transfer and balance the adsorption-desorption of intermediates during reaction process.<sup>30</sup> However, in specific conditions, it is necessary to consider carefully the role of O<sub>V</sub> and intrinsic properties of as-synthesize materials in catalytic performance.

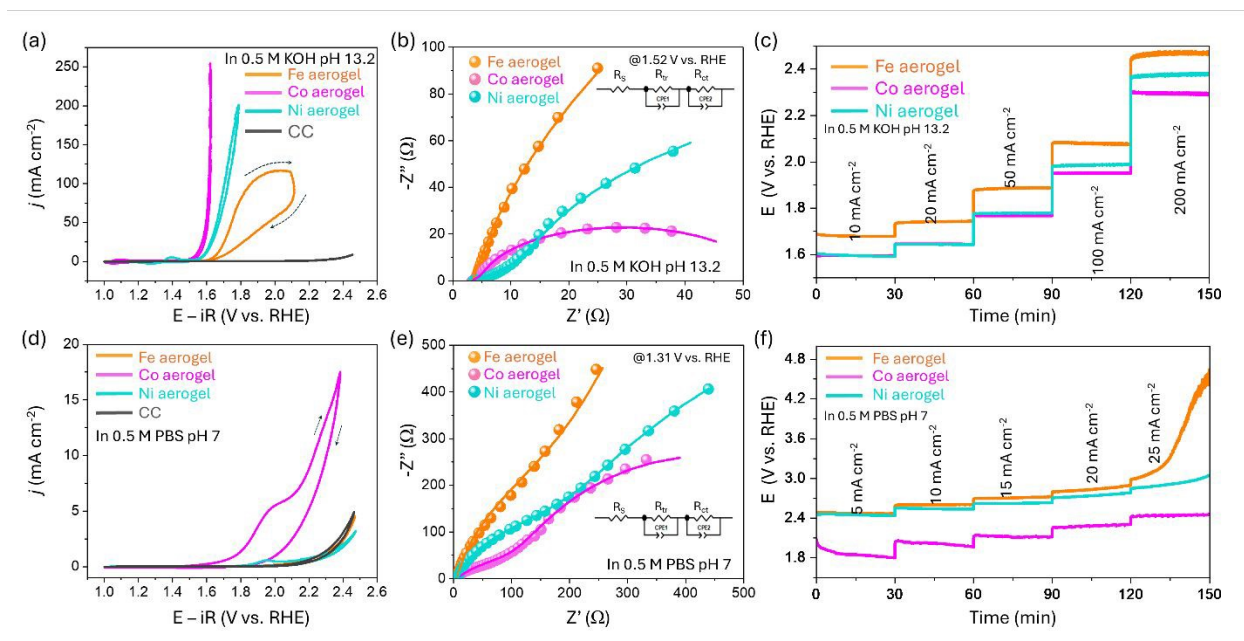


**Figure 3.** Anodic OER electrocatalytic performance of as-prepared catalysts: iR-corrected CV ( $v = 5 \text{ mV s}^{-1}$ ; 3<sup>rd</sup> scan) in (a) 0.5 M KOH (pH = 13.2) and (d) 0.5 M PBS (pH = 7); Nyquist plots of the EIS data collected (b) at 1.52 V vs. RHE in 0.5 M KOH and (e) at 1.31 V vs. RHE in 0.5 M PBS; short-term CP collected at different current densities in (c) 0.5 M KOH and (f) 0.5 M PBS.

To elucidate the intrinsic electrocatalytic activity of the as-prepared catalysts, electrochemical measurements for anodic OER and cathodic HER were conducted using a standard three-electrode configuration in 0.5 M KOH and 0.5 M PBS, serving as alkaline and neutral electrolytes, respectively. As illustrated in **Figure 3a**, iR-corrected OER polarization curves recorded in alkaline electrolyte show that Co aerogel requires an overpotential of only 383 mV to achieve a current density of  $100 \text{ mA cm}^{-2}$ . This value is significantly lower than those of Ni aerogel (475 mV) and Fe aerogel (630 mV), demonstrating the superior alkaline cathodic OER performance of Co aerogel among investigated catalysts. Besides that, alkaline cathodic OER catalytic activity of CC substrate is exceptionally minimal, suggesting that CC substrate contributes negligibly to the overall alkaline cathodic OER performance. Subsequently, EIS measurements were performed to investigate the electron transfer kinetics of the as-prepared catalysts. The equivalent circuit model used for Nyquist plot fitting is presented in **Figure S3** (SI) which includes uncompensated solution resistance ( $R_s$ ), internal charge transport resistance within the catalyst electrode ( $R_{tr}$ ), interfacial charge-transfer resistance between the electrode and electrolyte ( $R_{ct}$ ), and a constant phase element (CPE).<sup>31</sup> According to the fitting results, Nyquist plots obtained under alkaline cathodic OER conditions (**Figure 3b**) reveal that Co aerogel exhibits the smallest  $R_{ct}$  (98  $\Omega$ ), markedly lower than those of Ni aerogel (189  $\Omega$ ) and Fe aerogel (7855  $\Omega$ ), indicating a more efficient charge-transfer process in Co aerogel. The corresponding Nyquist fitting parameters are summarized in **Table S2** (SI). Furthermore, short-term CP tests conducted at different current densities indicate



no noticeable performance degradation in short duration was observed, even at high current densities of 100 and 200 mA cm<sup>-2</sup>, demonstrating that all as-prepared catalysts exhibit promising stability under alkaline anodic OER conditions (**Figure 3c**). Furthermore, Ni and Co aerogels exhibit comparable voltage requirements at low current densities ( $j = 10, 20, \text{ and } 50 \text{ mA cm}^{-2}$ ). However, at higher current densities ( $j = 100 \text{ and } 200 \text{ mA cm}^{-2}$ ), Co aerogel outperforms Ni aerogel by requiring a lower applied potential to deliver the same current. In contrast, Fe aerogel consistently demands substantially higher working potentials to reach comparable current densities, indicating the poorest catalytic activity among synthesized aerogels. Compared to those catalysts, CC exhibits poor short-time performance, suggesting its unstable activity (**Fig. S4a, SI**).

Subsequently, the 3<sup>rd</sup> CV polarization curves of the as-prepared catalysts and CC under neutral anodic OER conditions are shown in **Figure 3d**. The results indicate that only Co aerogel exhibits discernible anodic OER activity in a neutral electrolyte, whereas Fe and Ni aerogels show inactive catalytic activity, as their current densities overlap with those of bare CC substrate. As presented in **Figure 3e**, obtained Nyquist plot and fitting curves demonstrated that the smallest semicircle radius belongs to Co aerogel, reflecting the most favorable charge transfer of Co aerogel. The Nyquist fitted parameters of as-prepared catalysts for neutral cathodic OER are listed in **Table S3, SI**. Short-term CP measurements confirm the high stability of Co aerogel, which exhibits negligible current decay during the tests (**Figure 3f**). Conversely, Fe aerogel and CC substrate exhibit the aggressive demands on energy consumption (**Figure S4b, SI**), due to their poor catalytic activities.



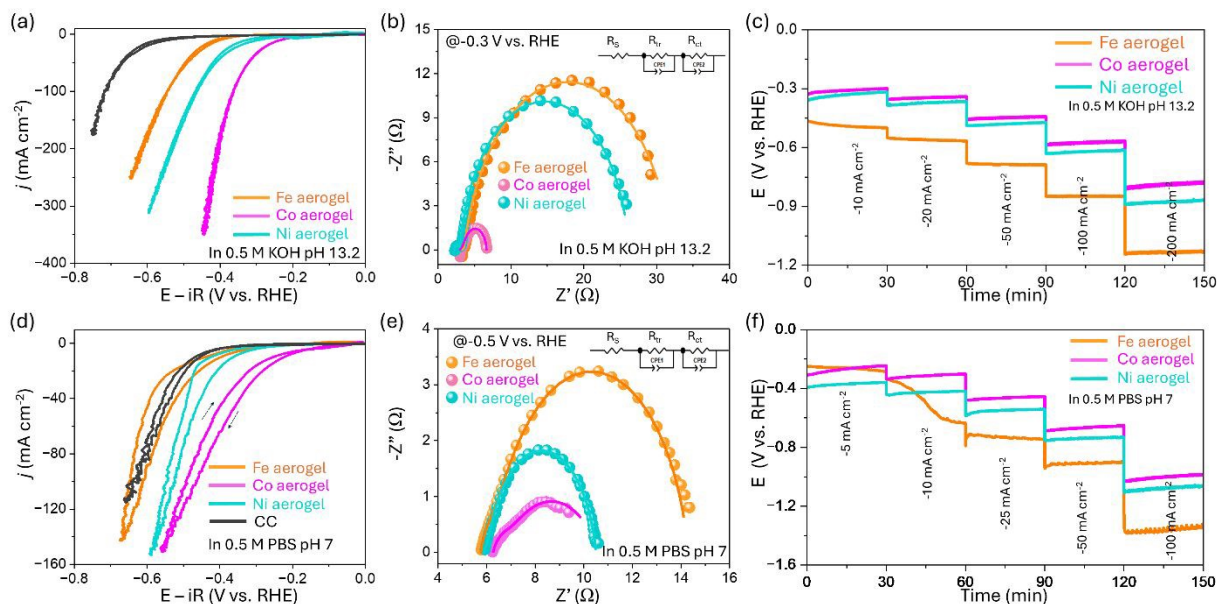


**Figure 4.** The cathodic HER electrocatalytic performance of as-prepared catalysts: Cyclic voltammograms ( $v = 5 \text{ mV s}^{-1}$ ; 3<sup>rd</sup> scan) in (a) 0.5 M KOH (pH = 13.2) and (d) 0.5 M PBS (pH = 7); Nyquist plots of the EIS data collected (b) at -0.3 V vs. RHE in 0.5 M KOH and (e) at -0.5 V vs. RHE in 0.5 M PBS; short-term CP collected at different current densities in (c) 0.5 M KOH and (f) 0.5 M PBS.

The electrocatalytic anodic HER performance of as-prepared aerogels was first evaluated under alkaline condition. As shown by the  $iR$ -corrected polarization curves in **Figure 4a**, overpotentials required to reach a current density of  $100 \text{ mA cm}^{-2}$  are 526 mV for Fe aerogel, 365 mV for Co aerogel, and 463 mV for Ni aerogel. These results demonstrate that Co aerogel exhibits superior alkaline cathodic HER catalytic activity compared with Fe and Ni aerogels. Moreover, the current density delivered by CC is substantially lower than those of the as-synthesized catalysts within the same working potential window, indicating that the observed alkaline cathodic HER activity predominantly arises from the intrinsic catalytic properties of the synthesized materials. As



illustrated in Figure 4b, Nyquist plot and corresponding fitted curves of the as-prepared aerogels exhibit similar semicircular shape but markedly different radii. The Nyquist fitting parameters for alkaline cathodic HER, summarized in **Table S4 (SI)**, reveal that Co aerogel exhibits a relatively low  $R_{ct}$  (2.89  $\Omega$ ), which is significantly smaller than those of Ni aerogel (23.15  $\Omega$ ) and Fe aerogel (28.55  $\Omega$ ), suggesting the favorable charge transfer of Co aerogel. In addition, under alkaline cathodic HER condition, Ni and Co aerogels maintain good short-term stability across the entire range of tested current densities, whereas the performance of Fe aerogel and CC substrate deteriorate significantly due to inevitable corrosion at high required potentials (**Figure 4c** and **Figure S4c, SI**). These observations indicate that all as-prepared catalysts exhibit alkaline cathodic HER activity, with Co aerogel demonstrating the highest overall performance among the synthesized materials.

As shown in **Figure 4d**, neutral cathodic HER catalytic activities of the as-prepared catalysts and CC substrate were evaluated in 0.5 M PBS where Fe, Co, and Ni aerogels require overpotentials of 623, 464, and 526 mV, respectively, to achieve a current density of 100 mA cm<sup>-2</sup>. The relatively high overpotentials observed indicate sluggish cathodic HER kinetics in neutral media, which can be attributed to the limited availability of protons and hydroxide ions. The overlap of current densities of Fe aerogel and CC substrate highlights the non-catalytic activities of Fe aerogel. To further evaluate interfacial charge-transfer resistance  $R_{ct}$  of the as-prepared catalysts under neutral conditions, EIS measurements were performed in 0.5 M PBS at -0.5 V vs. RHE, revealing a single semicircular feature for all samples (**Figure 4e**). As a result, Co aerogel proves the lowest  $R_{ct}$  (3.9  $\Omega$ ), which is slightly lower than that of Ni aerogel (3.97  $\Omega$ ) and substantially lower than that of Fe aerogel (7.85  $\Omega$ ) (**Table S5, SI**), suggesting that Co aerogel possesses the fastest electron-transfer rate and more favorable interfacial reaction kinetics among mentioned aerogels. As shown in



**Figure 4f**, neutral cathodic HER short-term stability tests were performed at various cathodic current densities ranging from 5 to 100 mA cm<sup>-2</sup>. Particularly, Co and Ni aerogels exhibit minimal potential variations even at a high current density of -100 mA cm<sup>-2</sup>, whereas Fe aerogel degrades early at a low current density of -10 mA cm<sup>-2</sup> and demands significantly high potentials in subsequent current densities. These results demonstrate the high stability of Co and Ni aerogels under neutral cathodic HER conditions. The poor short-term stability of the CC substrate under neutral cathodic HER conditions is illustrated in **Figure S4d (SI)**. The alkaline/neutral anodic OER and cathodic HER CV curves of as-synthesized catalysts without iR correction are presented in **Figure S5 (SI)**.

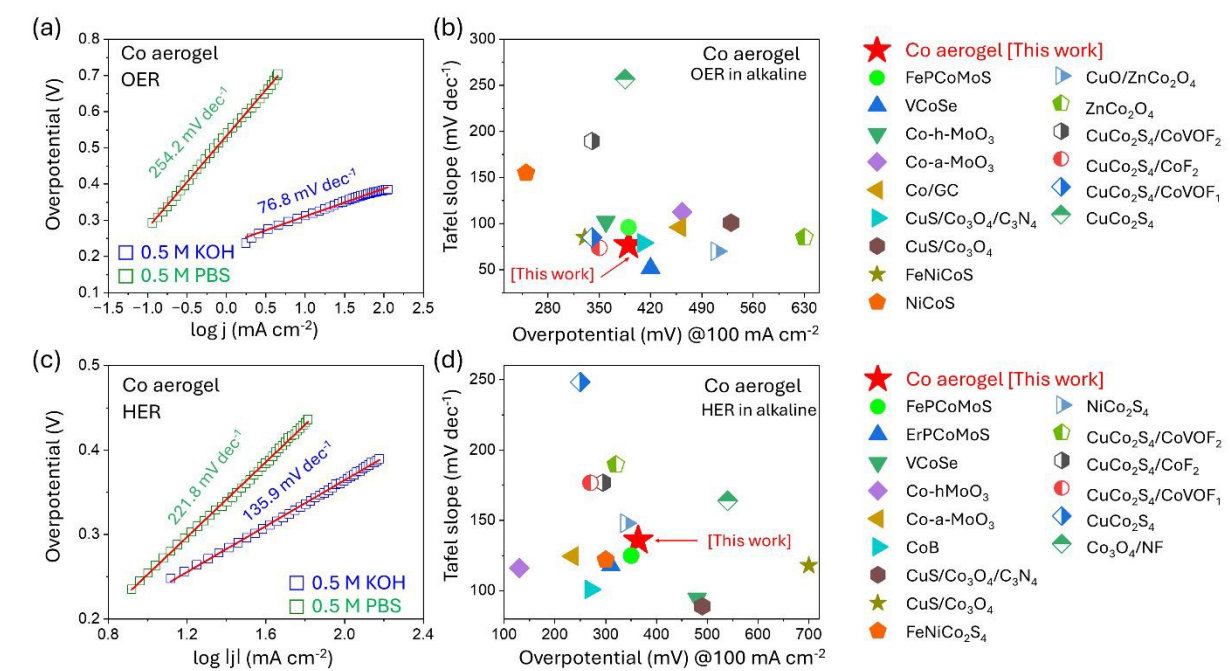


**Figure 5.** (a) Anodic OER Tafel slopes of Co aerogel in neutral and alkaline electrolytes, (b) Performance comparison in Tafel slope and overpotential at  $j = 100 \text{ mA cm}^{-2}$  of different reported Co-based catalysts for anodic OER performance in alkaline environment (See detailed information in Tabel S6, SI). (c) Cathodic HER Tafel slope of Co aerogel in neutral and alkaline electrolytes, (e) Performance comparison in Tafel slope and overpotential at  $j = 100 \text{ mA cm}^{-2}$  of different reported Co-based catalysts for cathodic HER performance in alkaline environment (See detailed information in Tabel S7, SI).

To further compare the electrocatalytic activity in alkaline and neutral media, the Tafel slopes of the best-performing catalyst, Co aerogel, were derived. As shown in **Figure 5a**, Co aerogel exhibits a substantially lower anodic OER Tafel slope in alkaline electrolyte ( $76.8 \text{ mV dec}^{-1}$ ) than in neutral electrolyte ( $254.2 \text{ mV dec}^{-1}$ ), indicating more favorable anodic OER kinetics under alkaline conditions. Tafel slopes of all as-prepared catalysts in neutral and alkaline environments are illustrated in **Figure S6** (SI). We note, however, that Tafel analysis for Fe aerogel in neutral HER - and for Fe and Ni aerogels in neutral OER - is not physically meaningful, as their polarization curves overlap with those of the bare CC substrate (**Figures 3d** and **4d**), confirming the absence of intrinsic electrocatalytic activity. In comparison in Tafel slope and overpotential at  $j = 100 \text{ mA cm}^{-2}$  of anodic OER performance in alkaline environment to other reported Co-based catalysts, Co aerogel exhibits promising anodic OER performance even though using the lower concentration of electrolyte (**Figure 5b** and **Table S6, SI**). Additionally, cathodic HER kinetic is explored as shown in **Figure 5c** which Co aerogel exhibits a lower Tafel slope in alkaline electrolyte ( $135.9 \text{ mV dec}^{-1}$ ) than in neutral electrolyte ( $221.8 \text{ mV dec}^{-1}$ ), further confirming its more favorable cathodic HER kinetics under alkaline conditions compared with neutral media.<sup>32</sup> Subsequently, cathodic HER performance of Co aerogel via Tafel slope and overpotential at  $j = -$



100 mA cm<sup>-2</sup> in alkaline environment demonstrates the acceptance performance compared in state-of-the-art Co-based catalysts (**Figure 5d** and **Table S7, SI**).

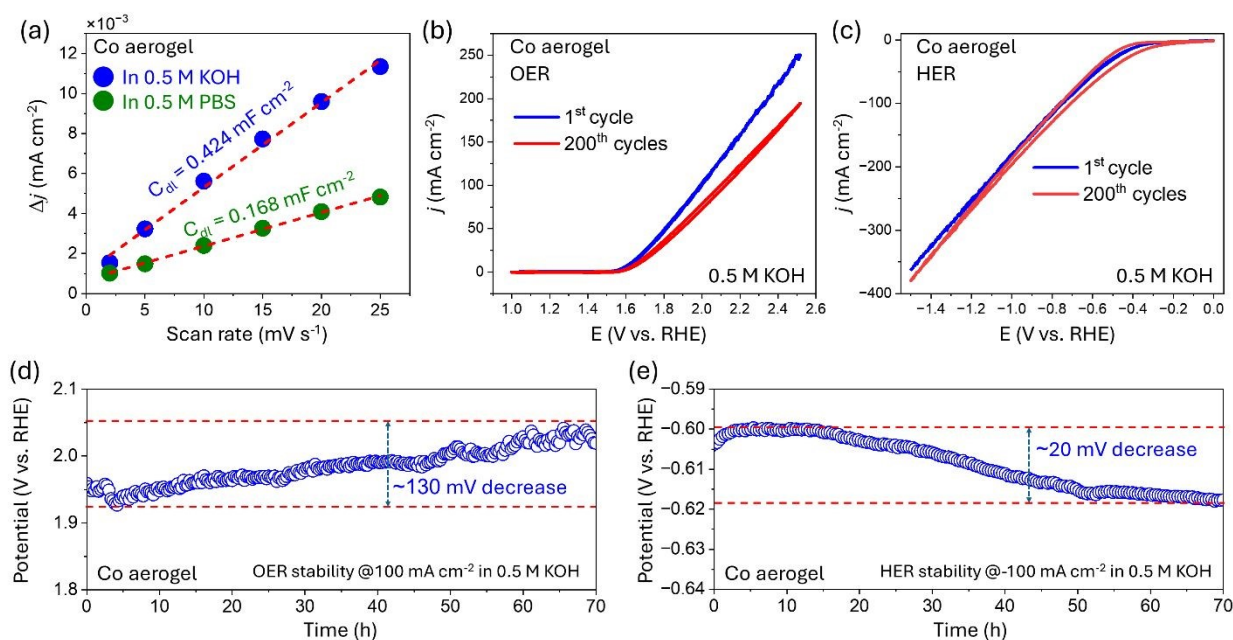


**Figure 6.** (a)  $C_{dl}$  values of Co aerogel in neutral and alkaline environments. Long-term stability before and after 200 CV cycles (scan rate:  $5 \text{ mV s}^{-1}$ ) of (b) anodic OER in 0.5 M KOH and (c) cathodic HER in 0.5 M KOH. Time-dependent CP curves of Co aerogel d) in anodic OER 0.5 M KOH and e) in cathodic HER 0.5 M KOH.

To assess the electrochemically active surface areas (ECSA) of the as-synthesized catalysts, the electrochemical double-layer capacitance ( $C_{dl}$ ) was obtained. As shown in **Figure S7-S8 (SI)**,  $C_{dl}$  values were derived from CV curves recorded in the non-Faradaic region at various scan rates ( $2-25 \text{ mV s}^{-1}$ ). Notably, all catalysts show higher ECSA values in 0.5 M KOH than those measured in 0.5 M PBS (**Figure S9, SI**). This variance is fundamentally attributed to the difference in the  $C_{dl}$  of the electrode-electrolyte interfaces. The smaller hydrated radii and strong specific adsorption of  $\text{OH}^-$  ions in KOH lead to a higher  $C_{dl}$  compared to the bulkier phosphate anions in PBS.



Therefore, the ECSA values in this study are primarily utilized to compare the relative electrochemically active surface areas among different catalysts within the same electrolyte medium, rather than making cross-electrolyte absolute ECSA comparisons. Using a nominal  $C_s$  value of  $40 \mu\text{F cm}^{-2}$  for this relative estimation ( $\text{ECSA} = C_{\text{dl}}/C_s$ ), the calculated ECSA values under alkaline conditions follow the order: Co aerogel ( $30.5 \text{ cm}^2$ ) > Ni aerogel ( $27.0 \text{ cm}^2$ ) > Fe aerogel ( $10.6 \text{ cm}^2$ ). A similar trend is observed under neutral conditions: Co aerogel ( $4.2 \text{ cm}^2$ ) > Ni aerogel ( $4.1 \text{ cm}^2$ ) > Fe aerogel ( $2.4 \text{ cm}^2$ ) (**Figure S9, SI**). These results consistently indicate that the Co aerogel possesses a higher density of electrochemically accessible active sites than the Ni and Fe aerogels, regardless of the examined electrolyte.

Aside from the catalytic activity, the long-term durability of the Co aerogel in alkaline cathodic HER and alkaline anodic OER was assessed by sequential CV sweeps at a scan rate of  $5 \text{ mV s}^{-1}$ . As exhibited in **Figure 6b-c**, alkaline cathodic OER CV curves of Co aerogel show a slight deterioration whereas in alkaline cathodic HER, the current densities remained almost unchanged after 200 cycles. To further assess the long-term stability of the Co aerogel for HER and OER, a 70-h CP analysis was conducted within a three-electrode system. In **Figure 6d**, the lowest overpotential for anodic OER is measured as 697 mV (without iR correction) at current density of  $100 \text{ mA cm}^{-2}$ . Over time, this overpotential shows an increase to 130 mV after 70 h, which can be attributed to a combination of intrinsic material properties and the extrinsic limitations of the batch-type testing system. Intrinsically, the amorphous nature of the aerogel, while providing abundant active defect sites, is thermodynamically metastable and thus more prone to structural degradation or surface reconstruction under harsh continuous polarization compared to its crystalline counterparts. Extrinsically, the vigorous evolution of  $\text{O}_2$  and  $\text{H}_2$  gases at  $100 \text{ mA cm}^{-2}$  and  $-100 \text{ mA cm}^{-2}$  in turn leads to severe bubble accumulation on the electrode surface, physically



blocking active sites and increasing mass-transport resistance.<sup>33</sup> Additionally, testing in an undivided batch cell without pH correction inevitably results in local and bulk pH fluctuations over time, which further contributes to the apparent increase in the measured potential.<sup>34</sup> In contrast, for the cathodic HER process (**Figure 6e**), the overpotential at  $j = -100 \text{ mA cm}^{-2}$  remains nearly constant, exhibiting only a 20 mV decrease after 70 h, which indicates excellent stability of the Co aerogel electrode during HER.

#### 4. Conclusion

In summary,  $\text{O}_V$ -rich 3d-VIIIB-metal aerogels with an amorphous main phase and highly porous structure were rapidly synthesized by a one-step reduction method under ambient conditions. Among them, obtained Co aerogel displays the highest anodic OER and cathodic HER electrocatalytic activity and durability, achieving remarkably low overpotentials for alkaline OER and HER of 383 mV and 365 mV at  $j = 100 \text{ mA cm}^{-2}$ , respectively. It is observed that the alkaline environment can effectively enhance the OER and HER activities compared to neutral one. Due to the highest  $\text{O}_V$  percentage and favorable intrinsic properties for electrocatalytic activity, Co aerogel presents an OER Tafel slope of  $254.2 \text{ mV dec}^{-1}$  and an HER Tafel slope of  $135.9 \text{ mV dec}^{-1}$  in alkaline conditions, which are comparable to those of previously reported Co-based catalysts. Even though possessing a high  $\text{O}_V$  content, Fe and Ni aerogels are electrochemically inactive or exhibit negligible activity in neutral electrolyte. Therefore, this study provides insights into the crucial role of intrinsic properties in catalytic activity over that of oxygen vacancies. Furthermore, this study presents the electrochemical OER and HER behaviors of  $\text{O}_V$ -rich 3d-VIIIB-metal aerogels featuring highly efficient and facile synthesis; subsequently, it suggests a readily scalable



synthesis route for O<sub>V</sub>-rich Co aerogel as a promising candidate for practical water-splitting electrocatalysts.

### **Conflicts of interest**

There are no conflicts to declare.

### **Data availability**

The data supporting this article have been included as part of the supplementary information (SI).

### **Author contributions statements**

T.K.C.P: Conceptualization, methodology, investigation, formal analysis, writing – original draft, writing – review & editing; N.T.N: Investigation, formal analysis, writing – original draft, writing – review & editing; N.N.L: Resources, supervision, formal analysis, writing – review & editing; P.L.N: Resources, Supervision, formal analysis, writing – review & editing; T.V.B.P: Resources, funding acquisition, project administration, supervision.

### **Acknowledgments**

The authors sincerely acknowledge the financial support provided by the VinUniversity Innovation Fund and Seed Grant.



## References

- 1 Y. Liu, Y. Wang, P. Fornasiero, G. Tian, P. Strasser and X. Y. Yang, *Angew. Chem. Int. Ed.*, 2024, **63**, e202412087.
- 2 G. Yang, D. Fang, Y. Lin, W. Wang, Y. Fu, D. Gao, Y. Mao, X. Wang and J. Li, *J. Mater. Chem. A Mater.*, 2025, **13**, 17920–17931.
- 3 X. Wang, Y. Fei, W. Wang, W. Yuan and C. M. Li, *ACS Appl. Energy Mater.*, 2019, **2**, 8851–8861.
- 4 M. Zhao, T. Li, L. Jia, H. Li, W. Yuan and C. M. Li, *ChemSusChem*, 2019, **12**, 5041–5050.
- 5 F. Wang, L. Xiao, Y. Jiang, X. Liu, X. Zhao, Q. Kong, A. Abd McKayum and G. Hu, *Mater. Horiz.*, 2025, **12**, 1757–1795.
- 6 G. Singla, M. Mahajan, S. N. Bhange and V. Kashyap, *New Journal of Chemistry*, 2025, **49**, 10056–10064.
- 7 D. N. Nguyen, T. K. C. Phu, J. Kim, W. T. Hong, J. S. Kim, S. H. Roh, H. S. Park, C. H. Chung, W. S. Choe, H. Shin, J. Y. Lee and J. K. Kim, *Small*, 2022, **18**, 2204797.
- 8 T. M. Pham, N. Liu, S. Bartling, N. Rockstroh, R. Eckelt, W. Ju, A. E. Surkus and R. Francke, *J. Catal.*, 2025, **450**, 116299.
- 9 E. Sadeghi, S. Chamani, I. D. Yildirim, E. Erdem, N. S. Peighambaroust and U. Aydemir, *ACS Appl. Mater. Interfaces*, 2024, **16**, 10078–10092.



- 10 E. Sadeghi, S. Chamani, E. Erdem, N. S. Peighamardoust and U. Aydemir, *ACS Appl. Energy Mater.*, 2023, **6**, 7658–7671.
- 11 X. Wang, H. Tian, X. Yu, L. Chen, X. Cui and J. Shi, *Chinese Journal of Catalysis*, 2023, **51**, 5–48.
- 12 L. Wei, F. Yang, W. Cai and L. Feng, *Energy & Fuels*, 2025, **39**, 14007–14027.
- 13 D. Guo, H. Xia, X. Guo, L. Wen, T. Wang, X. Li and Z. Sun, *Int. J. Hydrogen Energy*, 2024, **79**, 73–85.
- 14 Y. Fu, Y. Liu, G. Jin, H. Guo, H. Liu and C. Wang, *ACS Sustain. Chem. Eng.*, 2025, **13**, 8580–8591.
- 15 J. Liang, X. Wu, J. Ma, J. Huang, J. Wu, R. Zhong, Z. Zou, Y. Hou, Q. Wang and X. Zheng, *ACS Sustain. Chem. Eng.*, 2025, **13**, 15747–15761.
- 16 D. P. Sahoo, U. A. Mohanty, K. Kumar Das, R. Mohanty and K. Parida, *Mater. Adv.*, DOI:10.1039/d5ma01125f.
- 17 S. Mishra, B. L. Tudu, N. Mishra, K. Sanjay and R. Acharya, *Mater. Adv.*, 2025, **6**, 9085–9103.
- 18 T. K. C. Phu, T. N. Pham, T. D. Nguyen, A. G. Nguyen, T. N. Tran, N. N. Le, P. L. Nguyen and T. V. B. Phung, *Mater. Chem. Front.*, 2025, **9**, 3174–3187.
- 19 Y. Wang, L. Cheng, Y. Zhu, J. Liu, C. Xiao, R. Chen, L. Zhang, Y. Li and C. Li, *Appl. Catal. B*, 2022, **317**, 121650.
- 20 X. Wang, C. Xing, Z. Liang, P. Guardia, X. Han, Y. Zuo, J. Llorca, J. Arbiol, J. Li and A. Cabot, *J. Mater. Chem. A Mater.*, 2022, **10**, 3659–3666.



- 21 Y. Yang, L. Zhuang, T. E. Rufford, S. Wang and Z. Zhu, *RSC Adv.*, 2017, **7**, 32923–32930.
- 22 F. Bai, Y. He, L. Xu, Y. Wang, Y. Wang, Z. Hao and F. Li, *RSC Adv.*, 2022, **12**, 2408–2415.
- 23 Z. Li, D. Liu, Y. Cai, Y. Wang and J. Teng, *Fuel*, 2019, **257**, 116031.
- 24 X. Du, J. Zhang, M. Zhang, H. Wei, X. Lin, W. Guo, P. Zhang and Z. Luo, *Green Chemistry*, 2025, **27**, 7380–7388.
- 25 X. Zhang, S. Ding, Q. Shen, S. Feng, J. Li, Z. Sun, C. Lei, J. Xue and M. Liu, *J. Mater. Chem. A Mater.*, 2025, **13**, 13872–13883.
- 26 B. Sirichandana, R. Silviya, S. V. Bhat, N. Patel and G. Hegde, *Nanoscale Adv.*, 2025, **7**, 4056–4066.
- 27 X. Tao, X. Wang, C. Yang, M. Zhao, C. Wang, C. Zhang, J. Lu, S. Zhang, R. Ma and C. Guo, *Chemical Engineering Journal*, 2025, **524**, 169448.
- 28 T. K. C. Phu, W. T. Hong, H. Han, Y. I. Song, J. H. Kim, S. H. Roh, M. C. Kim, J. H. Koh, B. K. Oh, J. Y. Kim, C. H. Chung, D. H. Lee and J. K. Kim, *Materials Today*, 2024, **76**, 52–63.
- 29 J. Y. Kim, W. T. Hong, T. K. C. Phu, S. C. Cho, B. Kim, U. Baeck, H. S. Oh, J. H. Koh, X. Yu, C. H. Choi, J. Park, S. U. Lee, C. H. Chung and J. K. Kim, *Advanced Science*, 2024, **11**, 2405154.
- 30 N. Luo, A. Cai, J. Pei, X. Zeng, X. Wang and N. Yao, *Adv. Funct. Mater.*, 2025, **35**, 2425503.



- 31 T. K. C. Phu, T. N. Pham, A. G. Nguyen, T. N. Tran, T. M. A. Tran, N. N. Le, P. L. Nguyen and T. V. B. Phung, *iScience*, 2025, **28**, 112729.
- 32 T. K. C. Phu, N. N. Le, T. N. Tran, T. T. T. Vuong, H. D. Nguyen, T. V. B. Phung, P. A. Le and P. L. Nguyen, *ACS Appl. Energy Mater.*, 2024, **7**, 10938–10949.
- 33 Y. H. Liu, F. Y. Zeng, Y. S. Kuo, Y. Chen and C. L. Hsu, *J. Mater. Chem. A Mater.*, 2025, **13**, 24062–24072.
- 34 T. M. Pham, M. Plevova, S. Bartling, N. Rockstroh, A. Springer, A. Slabon, J. Hnat, A. E. Surkus and R. Francke, *J. Catal.*, 2024, **438**, 115675.



The data supporting this article have been included as part of the Supplementary Information. Supplementary information: Raw data of TEM, FE-SEM, XRD and BET characterization. Experimental details and further electrochemical tests. See DOI: [10.5281/zenodo.19103624]

